

# Enhancing Remote Magnon-Magnon Entanglement with Quantum Interference

Yuan Gong,<sup>1</sup> Yan-Xue Cheng,<sup>1</sup> Wei Xiong,<sup>1,2,\*</sup> and Jiaojiao Chen<sup>1,†</sup>

<sup>1</sup>*Department of Physics, Wenzhou University, Zhejiang 325035, China*

<sup>2</sup>*International Quantum Academy, Shenzhen, 518048, China*

(Dated: November 18, 2025)

Cavity magnonics, owing to its strong magnon-photon coupling and excellent tunability, has attracted significant interest in quantum information science. However, achieving strong and robust macroscopic entanglement remains a long-standing challenge due to the inherently linear nature of the beam-splitter interaction. Here, we propose an experimentally feasible scheme to generate and enhance macroscopic entanglement between two remote magnon modes by injecting squeezed vacuum fields (SVFs) into coupled microwave cavities. We demonstrate that even a single SVF applied to one cavity can induce steady magnon-magnon entanglement, while applying two SVFs (the double-squeezed configuration) enables selective activation of two independent entanglement channels associated with the cavity supermodes. Remarkably, quantum interference between the two SVFs allows for phase-controlled enhancement of entanglement, resulting in significantly improved robustness against cavity dissipation and thermal noise. Under realistic parameters, the survival temperature of quantum entanglement increases from approximately 260 mK to 450 mK. Our results establish a versatile and controllable approach to generating and enhancing quantum entanglement through double-squeezed-field interference, opening new avenues to study and enhance macroscopic quantum physics in cavity-magnon systems with only beam-splitter interactions.

## I. INTRODUCTION

Magnons, the quanta of spin waves, are collective excitations of spin ensembles in magnetically ordered materials [1, 2]. Thanks to their high spin density and low damping [3], magnons in yttrium-iron-garnet (YIG) spheres have attracted considerable interest, both theoretically and experimentally, in quantum information science and spintronics [4, 5]. Benefiting from these unique properties, magnons can be coupled to diverse quantum systems, such as microwave photons [6], superconducting qubits [7], and phonons [8]. As a result, versatile hybrid quantum systems are constructed. As a typical magnon-based hybrid system, cavity magnonics [4] is established by magnons strongly coupled to microwave photons in a microwave cavity and has witnessed remarkable progress over the past decade, including dark modes [9], non-Hermitian dynamics [10–15], spin current [16], level attraction [17, 18], near-perfect absorption [19], and quantum magnon [20, 21]. It is evident that these novel phenomena are beneficial to the linear beam-splitter magnon-photon interaction in cavity magnonics. However, relying solely on such a coupling mechanism is extremely unfavorable for realizing macroscopic quantum entanglement [22], which is not only essential for quantum information processing [23] but also for probing the boundary between classical and quantum physics [24]. Therefore, generating macroscopic quantum entanglement in cavity magnonics remains a long-standing challenge.

To address this challenge, one approach is to couple magnons to phonons via the nonlinear magnetostri-

tive interaction [25–28], analogous to the optomechanical coupling in cavity optomechanics [29]. In the linearized regime, the two-mode squeezing terms generate magnon-phonon entanglement, while the beam-splitter terms simultaneously cool the phonons to facilitate the observation of entanglement. Assisted by the beam-splitter magnon-photon interaction, the magnon-phonon entanglement can be transferred among photons, phonons, and magnons, enabling the preparation of arbitrary bipartite or tripartite entanglement under appropriate conditions [25]. An alternative strategy is to directly couple magnons to microwave photons in electromechanical systems, effectively implementing cavity-magnon optomechanics in the microwave regime [30, 31]. In such systems, macroscopic entanglement arises from radiation-pressure-like interactions between photons and phonons, a mechanism closely analogous to that in cavity magnomechanics. Another promising route is to exploit the intrinsic Kerr nonlinearity of magnons in YIG spheres [32], which originates from magnetocrystalline anisotropy [33] and has been demonstrated experimentally [34, 35]. Beyond quantum entanglement, the magnon Kerr nonlinearity can also be used to investigate other rich physics, including bistability [36] and multistability [37], magnon-mediated remote spin-spin strong coupling [38], spin-polariton [39] and phonon-polariton strong coupling [40], exponentially enhanced tripartite interactions [41], quantum phase transitions [42–44], nonreciprocal entanglement [30, 45, 46], nonreciprocal photon blockade [47], ground-state cooling [48], and ultrasensitive detection [49]. A further approach is to inject squeezed vacuum fields (SVFs) into cavities to squeeze photons [50–55]. The quantum correlations of the squeezed fields can then be transferred to magnons via the beam-splitter magnon-photon interaction. As a result, two nonlocal magnon modes in a cavity [53, 54],

\* xiongweiphys@wzu.edu.cn  
† jjchenphys@wzu.edu.cn

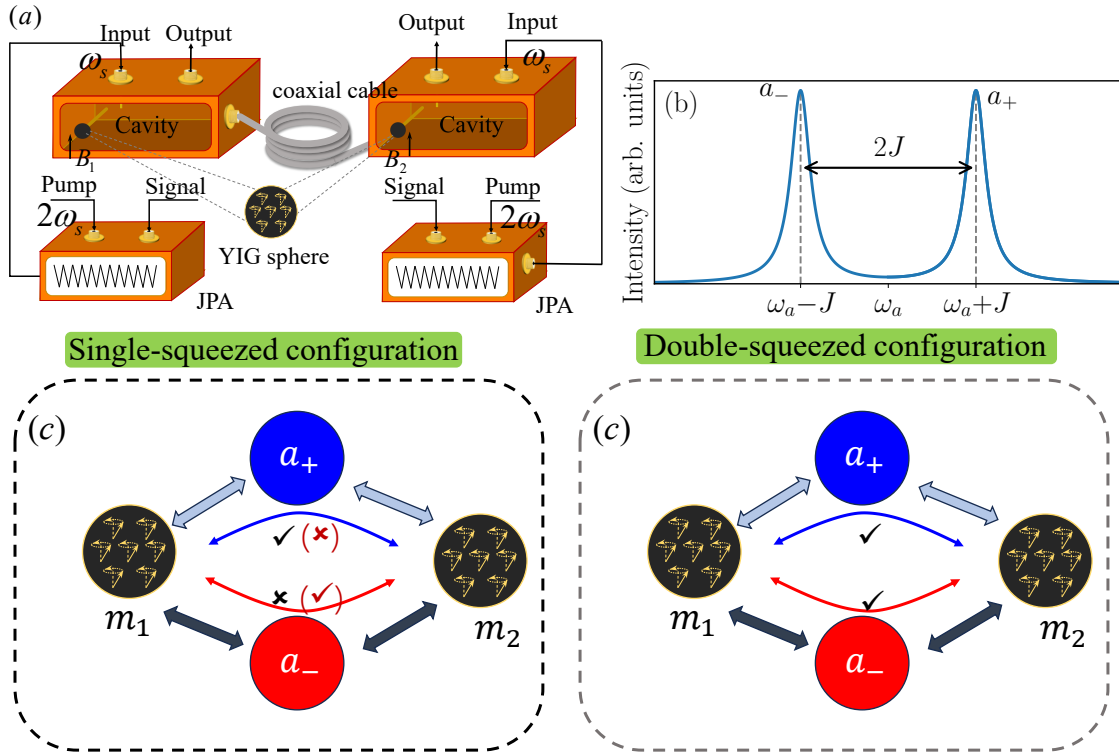


FIG. 1. (a) Schematic diagram of the coupled cavity-magnon system. Two microwave cavities, connected by a coaxial cable, are respectively driven by two single-mode squeezed vacuum fields with frequency  $\omega_s$ , generated by two Josephson parametric amplifiers (JPAs) pumped at frequency  $2\omega_s$ . (b) Two supermodes with frequencies  $\omega_a \pm J$ , formed by two resonant cavities, are depicted.  $2J$  is the separation between two supermodes. (c) The mechanism of the generation of the magnon-magnon entanglement in the single-squeezed configuration, where only one *determined* supermode can be activated. (d) The mechanism of the generation of the magnon-magnon entanglement in the double-squeezed configuration, where two supermode can be *selectively* activated, via tuning the detunings of the cavity.

magnons in uncoupled double cavities [52], and arbitrary pairs of remote magnon modes in a chain of cavity magnonics [55] can be entangled.

Building upon the squeezed vacuum field (SVF) approach, we propose an experimentally feasible scheme to not only generate but also enhance entanglement between two remote magnon modes. The system comprises two cavity modes coupled remotely via a coaxial cable [56], with each cavity mode coupled to a local magnon mode in a YIG sphere. We first demonstrate that magnon-magnon entanglement can be achieved using only a single SVF applied to one cavity mode, referred to as the single-squeezed configuration. In this case, the two supermodes formed from the strongly coupled cavity modes play an asymmetric role in mediating entanglement. Specifically, optimal entanglement arises only when the SVF is resonant with a *determined* supermode, implying that only one fixed entanglement channel is activated. We then consider the double-squeezed configuration, where a separate SVF drives each cavity mode. Here, both supermodes contribute equally to the generation of magnon-magnon entanglement. In contrast to the single-SVF case, optimal entanglement in this configuration can be achieved via either the upper or lower su-

permode by tuning the cavity detunings, indicating that two independent entanglement channels can be *selectively* activated. Moreover, we find that the two SVFs can interfere at the interface of one of the supermodes. When the SVFs are in phase, the magnon-magnon entanglement is significantly enhanced compared to the single-squeezed case. This interference provides an additional and promising path to coherent control of the degree of the entanglement via squeezing phases. Furthermore, the magnon-magnon entanglement exhibits enhanced robustness against cavity dissipation and elevated bath temperatures in the double-squeezed configuration. Under realistic parameters, the survival temperature for quantum entanglement is improved from approximately 260 mK in the single-squeezed configuration to about 450 mK in the double-squeezed case.

The remainder of this paper is organized as follows. In Sec. II, we give a brief introduction of the proposed system and the corresponding Hamiltonian and its dynamics are given. Then we show how to generate the magnon-magnon entanglement with a single SVF and enhance the entanglement with double SVFs in Sec. III. Finally, a summary is concluded in Sec. IV.

## II. MODEL AND QUANTUM LANGEVIN EQUATION

We consider a coupled cavity-magnon system, as illustrated in Fig. 1, composed of two YIG spheres and two microwave cavities connected via a coaxial cable. In each cavity, a YIG sphere is biased by a uniform static magnetic field to excite a magnon mode and is positioned near the region of maximum magnetic field to achieve strong coupling between the magnon mode and the cavity mode. Under the rotating-wave approximation, the total Hamiltonian can be written as (with  $\hbar = 1$ ):

$$H = H_0 + \sum_{j=1}^2 g_j (a_j m_j^\dagger + a_j^\dagger m_j) + J(a_1 a_2^\dagger + a_1^\dagger a_2), \quad (1)$$

where  $H_0 = \sum_{j=1,2} (\omega_{a_j} a_j^\dagger a_j + \omega_{m_j} m_j^\dagger m_j)$  is the free Hamiltonian, with  $\omega_{a_j}$  and  $\omega_{m_j}$  representing the resonance frequencies of the  $j$ th cavity and magnon modes, respectively. Here,  $a_j$  ( $a_j^\dagger$ ) and  $m_j$  ( $m_j^\dagger$ ) are the annihilation (creation) operators of the  $j$ th cavity and magnon modes,  $g_j$  denotes the coupling strength between the  $j$ th cavity mode and its embedded magnon mode, and  $J$  characterizes the intercavity coupling strength. This strong coupling gives rise to two supermodes with frequencies  $\omega_a \pm J$ , with separation  $2J$ , as illustrated in Fig. 1(b).

Including the dissipation of both cavity and magnon modes, the system dynamics are governed by the following quantum Langevin equations (QLEs) [57]:

$$\begin{aligned} \dot{a}_1 &= -(\kappa_{a_1} + i\omega_{a_1})a_1 - ig_1 m_1 - iJa_2 + \sqrt{2\kappa_{a_1}} a_1^{\text{in}}, \\ \dot{a}_2 &= -(\kappa_{a_2} + i\omega_{a_2})a_2 - ig_2 m_2 - iJa_1 + \sqrt{2\kappa_{a_2}} a_2^{\text{in}}, \\ \dot{m}_j &= -(\kappa_{m_j} + i\omega_{m_j})m_j - ig_j a_j + \sqrt{2\kappa_{m_j}} m_j^{\text{in}}, \end{aligned} \quad (2)$$

where  $\kappa_{a_j}$  and  $\kappa_{m_j}$  denote the decay rates of the  $j$ th cavity and magnon modes, respectively. The operators  $a_j^{\text{in}}$  and  $m_j^{\text{in}}$  represent the input noise operators for the  $j$ th cavity and magnon modes. These input noise operators have zero mean values and satisfy the correlation relations [57]:

$$\begin{aligned} \langle O_j^{\text{in},\dagger}(t) O_j^{\text{in}}(t') \rangle &= N_{O_j} \delta(t - t'), \quad O = a, m, \\ \langle O_j^{\text{in}}(t) O_j^{\text{in},\dagger}(t') \rangle &= (N_{O_j} + 1) \delta(t - t'), \end{aligned} \quad (3)$$

where  $N_{O_j} = [\exp(\hbar\omega_{O_j}/k_B T) - 1]^{-1}$  is the mean thermal occupation number, with  $T$  being the bath temperature and  $k_B$  the Boltzmann constant.

It is well known that the system with only beam-splitter interactions and input noise described by Eq. (3) cannot generate macroscopic entanglement [22]. To overcome this limitation, each cavity mode is driven by a single-mode squeezed vacuum field (SVF) instead of the original thermal noise (see Fig. 1), which can be readily generated via degenerate parametric down-conversion in flux-driven Josephson parametric amplifiers (JPAs) [58–67]. Experimentally, it has demonstrated that JPAs can achieve squeezing levels up to 10 dB [62]. When a JPA is pumped at frequency  $2\omega_s$  while its signal input port is kept in vacuum, it generates a squeezed microwave vacuum field centered at  $\omega_s$  (see Fig. 1) [63]. Alternatively, a squeezed vacuum field can also be realized using a degenerate parametric amplifier driven by a microwave pump [68]. In this double-squeezed configuration, the QLEs in Eq. (2) are modified as

$$\begin{aligned} \dot{a}_1 &= -(\kappa_{a_1} + i\Delta_{a_1})a_1 - ig_1 m_1 - iJa_2 + \sqrt{2\kappa_{a_1}} s_1^{\text{in}}, \\ \dot{a}_2 &= -(\kappa_{a_2} + i\Delta_{a_2})a_2 - ig_2 m_2 - iJa_1 + \sqrt{2\kappa_{a_2}} s_2^{\text{in}}, \\ \dot{m}_j &= -(\kappa_{m_j} + i\Delta_{m_j})m_j - ig_j a_j + \sqrt{2\kappa_{m_j}} m_j^{\text{in}}, \end{aligned} \quad (4)$$

where  $\Delta_{a_j} = \omega_{a_j} - \omega_s$  and  $\Delta_{m_j} = \omega_{m_j} - \omega_s$  are the detunings of the cavity and magnon modes from the SVF frequency  $\omega_s$ . The operators  $s_j^{\text{in}}$  denote the single-mode SVF acting on the  $j$ th cavity mode, satisfying [69]

$$\begin{aligned} \langle s_j^{\text{in},\dagger}(t) s_j^{\text{in}}(t') \rangle &= (N_{s_j}; N_{s_j} + 1) \delta(t - t'), \\ \langle s_j^{\text{in}}(t) s_j^{\text{in},\dagger}(t') \rangle &= (M_{s_j}; M_{s_j}^*) \delta(t - t'), \end{aligned} \quad (5)$$

where  $N_{s_j} = \sinh^2 r_j$  and  $M_{s_j} = e^{i\theta_j} \sinh r_j \cosh r_j$ , with  $r_j$  and  $\theta_j$  denoting the squeezing parameter and phase of the SVF acting on the  $j$ th cavity mode.

By introducing the quadrature operators for the cavity and magnon modes,  $x_{O_j} = (O_j^\dagger + O_j)/\sqrt{2}$ ,  $y_{O_j} = i(O_j^\dagger - O_j)/\sqrt{2}$ , Eq. (4) can be rewritten in the matrix form as

$$\dot{u}(t) = Au(t) + n(t), \quad (6)$$

where  $u(t) = [x_{a_1}, y_{a_1}, x_{a_2}, y_{a_2}, x_{m_1}, y_{m_1}, x_{m_2}, y_{m_2}]^T$ ,  $A$  is the drift matrix,

$$A = \begin{pmatrix} -\kappa_{a_1} & \Delta_{a_1} & 0 & J & 0 & g_1 & 0 & 0 \\ -\Delta_{a_1} & -\kappa_{a_1} & -J & 0 & -g_1 & 0 & 0 & 0 \\ 0 & J & -\kappa_{a_2} & \Delta_{a_2} & 0 & 0 & 0 & g_2 \\ -J & 0 & -\Delta_{a_2} & -\kappa_{a_2} & 0 & 0 & -g_2 & 0 \\ 0 & g_1 & 0 & 0 & -\kappa_{m_1} & \Delta_{m_1} & 0 & 0 \\ -g_1 & 0 & 0 & 0 & -\Delta_{m_1} & -\kappa_{m_1} & 0 & 0 \\ 0 & 0 & 0 & g_2 & 0 & 0 & -\kappa_{m_2} & \Delta_{m_2} \\ 0 & 0 & -g_2 & 0 & 0 & 0 & -\Delta_{m_2} & -\kappa_{m_2} \end{pmatrix}, \quad (7)$$

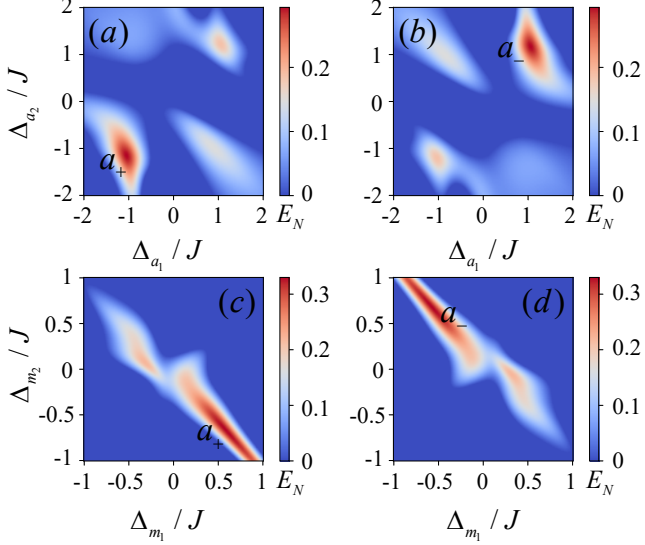


FIG. 2. The degree of magnon-magnon entanglement is shown as a function of (a, b) the normalized cavity detunings and (c, d) the normalized magnon detunings in the single-squeezed configuration. In panel (a), we take  $\Delta_{m_1} = -\Delta_{m_2} = 0.5J$ , while in panel (b),  $\Delta_{m_1} = -\Delta_{m_2} = -0.5J$ . In panel (c), the cavity detunings are fixed at  $\Delta_{a_1} = \Delta_{a_2} = -J$ , and in panel (d), they are fixed at  $\Delta_{a_1} = \Delta_{a_2} = J$ . Other parameters are chosen as in Ref. [70]:  $\kappa_{a_1}/2\pi = \kappa_{a_2}/2\pi = \kappa_a/2\pi = 5$  MHz,  $\kappa_{m_1} = \kappa_{m_2} = \kappa_a/5$ ,  $J = 4\kappa_a$ ,  $g_1 = g_2 = 2\kappa_a$ ,  $r_1 = r_2 = 0.9$ , and  $\theta_1 = \theta_2 = 0$ .

and  $n(t) = [\sqrt{2\kappa_{a_1}}x_{s_1}^{\text{in}}(t), \sqrt{2\kappa_{a_1}}y_{s_1}^{\text{in}}(t), \sqrt{2\kappa_{a_2}}x_{s_2}^{\text{in}}(t), \sqrt{2\kappa_{a_2}}y_{s_2}^{\text{in}}(t), \sqrt{2\kappa_{m_1}}x_{m_1}^{\text{in}}(t), \sqrt{2\kappa_{m_1}}y_{m_1}^{\text{in}}(t), \sqrt{2\kappa_{m_2}}x_{m_2}^{\text{in}}(t), \sqrt{2\kappa_{m_2}}y_{m_2}^{\text{in}}(t)]^T$  is the vector of input noises. Since the system dynamics are linear and the input noises are Gaussian, any Gaussian input state remains Gaussian, and the steady state of the system is therefore a continuous-variable four-mode Gaussian state, fully characterized by the  $8 \times 8$  covariance matrix  $V$ , defined as  $V_{pq}(t) = \frac{1}{2}\langle u_p(t)u_q(t') + u_q(t')u_p(t) \rangle$  ( $p, q = 1, 2, \dots, 8$ ).

In the long-time limit ( $t \rightarrow \infty$ ), the system reaches a stable steady state, and the covariance matrix  $V$  can be obtained by solving the Lyapunov equation [29]:

$$AV + VA^T = -D, \quad (8)$$

where  $D$  is the diffusion matrix, defined via

$$D_{pq}\delta(t - t') = \frac{1}{2}\langle n_p(t)n_q(t') + n_q(t')n_p(t) \rangle. \quad (9)$$

Specifically, it can be written as a direct sum

$$D = D_{s_1} \oplus D_{s_2} \oplus D_{m_1} \oplus D_{m_2}, \quad (10)$$

with

$$D_{s_j} = \kappa_{a_j} \begin{pmatrix} 2N_{s_j} + 1 + 2\text{Re}[M_{s_j}] & 2\text{Im}[M_{s_j}] \\ 2\text{Im}[M_{s_j}] & 2N_{s_j} + 1 - 2\text{Re}[M_{s_j}] \end{pmatrix}, \quad (11)$$

and

$$D_{m_j} = \kappa_{m_j} \text{Diag}[2N_{m_j} + 1, 2N_{m_j} + 1]. \quad (12)$$

Once the covariance matrix  $V$  is obtained, the bipartite entanglement between the two magnon modes can be quantified using the *logarithmic negativity* [71, 72]:

$$E_N \equiv \max[0, -\ln 2\eta^-], \quad (13)$$

with

$$\eta^- = 2^{-1/2} \left[ \Sigma - (\Sigma^2 - 4 \det V_{mm})^{1/2} \right]^{1/2}, \quad (14)$$

where  $\Sigma = \det A + \det B - 2 \det C$ , and

$$V_{mm} = \begin{pmatrix} A & C \\ C^T & B \end{pmatrix} \quad (15)$$

is the  $4 \times 4$  covariance submatrix associated with the two magnon modes [73]. Here,  $A$ ,  $B$ , and  $C$  are the  $2 \times 2$  blocks of  $V_{mm}$ . A positive logarithmic negativity, i.e.,  $E_N > 0$ , indicates the presence of bipartite entanglement between the two magnon modes.

### III. RESULTS AND DISCUSSION

We first demonstrate that magnon-magnon entanglement can be generated by driving only a single cavity mode with a single-mode squeezed vacuum field (SVF). Without loss of generality, we assume that the SVF is injected into cavity mode  $a_1$ . In this single-squeezed configuration, the input noise term  $s_2^{\text{in}}$  in Eq. (4) reduces

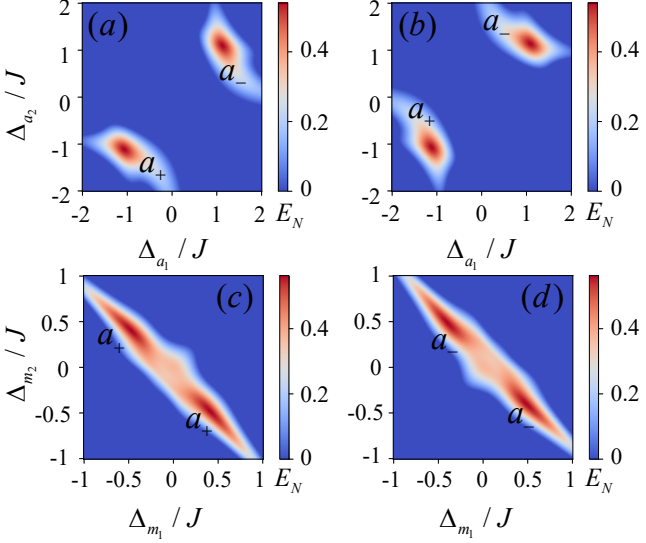


FIG. 3. The degree of magnon-magnon entanglement is shown as a function of (a, b) the normalized cavity detunings and (c, d) the normalized magnon detunings in the double-squeezed configuration. In panel (a), we take  $\Delta_{m_1} = -\Delta_{m_2} = 0.5J$ , while in panel (b),  $\Delta_{m_1} = -\Delta_{m_2} = -0.5J$ . In panel (c), the cavity detunings are fixed at  $\Delta_{a_1} = \Delta_{a_2} = -J$ , and in panel (d), they are fixed at  $\Delta_{a_1} = \Delta_{a_2} = J$ . Other parameters are the same as those in Fig. 2.

to the vacuum noise operator  $a_2^{\text{in}}$  from Eq. (2), and its correlation function reverts to the form given in Eq. (3). Consequently, the diffusion matrix  $D$  in Eq. (10) becomes

$$D = D_{s_1} \oplus D_{a_2} \oplus D_{m_1} \oplus D_{m_2}, \quad (16)$$

where  $D_{a_2} = \kappa_{a_2} \cdot \text{Diag}[2N_{a_2} + 1, 2N_{a_2} + 1]$ .

By numerically solving Eq. (8), we evaluate the degree of magnon-magnon entanglement. A key prerequisite is to identify the optimal detunings for the cavity and magnon modes that maximize entanglement. Figures 2(a) and 2(b) show the magnon-magnon entanglement as a function of the normalized cavity detunings, while the magnon detunings are fixed at  $\Delta_{m_1} = -\Delta_{m_2} = 0.5J$  and  $\Delta_{m_1} = -\Delta_{m_2} = -0.5J$ , respectively. Maximal entanglement occurs when  $\Delta_{a_1} = \Delta_{a_2} = \pm J$ , corresponding to the SVF being resonant with either the upper supermode  $a_+$  [Fig. 2(a)] or the lower supermode  $a_-$  [Fig. 2(b)]. This resonance allows efficient transfer of quantum correlations from the SVF to the magnon modes. Importantly, only one supermode is effectively activated to generate optimal entanglement, as further illustrated in Figs. 2(c) and 2(d), where entanglement is plotted against the normalized magnon detunings. This indicates only one entanglement channel is activated [see Fig. 1(c)]. In Fig. 2, the following experimental parameters are taken [70]:  $\kappa_{a_1}/2\pi = \kappa_{a_2}/2\pi = \kappa_a/2\pi = 5$  MHz,  $\kappa_{m_1} = \kappa_{m_2} = \kappa_a/5$ ,  $J = 4\kappa_a$ ,  $g_1 = g_2 = 2\kappa_a$ ,  $r_1 = r_2 = 0.9$ , and  $\theta_1 = \theta_2 = 0$ .

The magnon-magnon entanglement can be significantly enhanced by driving both cavity modes with

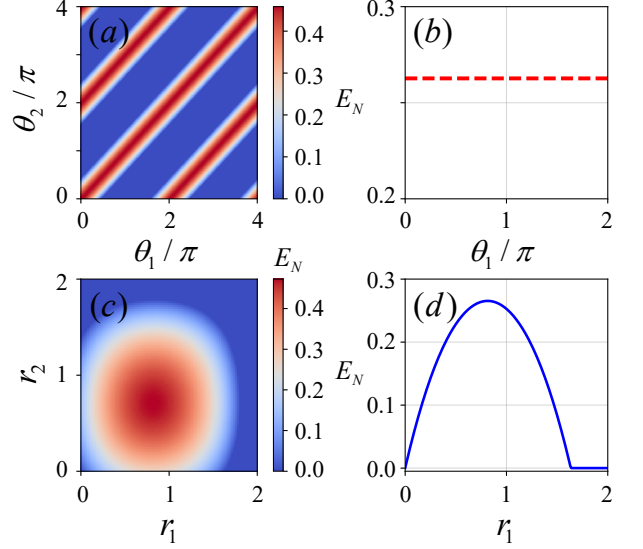


FIG. 4. The degree of magnon-magnon entanglement is plotted as a function of (a) the squeezing phases  $\theta_1$  and  $\theta_2$  in the double-squeezed configuration, (b) the squeezing parameter  $r_1$  in the single-squeezed configuration, (c) the squeezing parameters  $r_1$  and  $r_2$  in the double-squeezed configuration, and (d) the squeezing parameter  $r_1$  in the single-squeezed configuration. In panels (a) and (b), the squeezing phases are fixed at  $\theta_1 = \theta_2 = 0$ , while in panels (c) and (d), the squeezing strengths are set to  $r_1 = r_2 = 0.9$ . In all panels, the cavity detunings are fixed at  $\Delta_{a_1} = \Delta_{a_2} = -J$ , and the magnon detunings are chosen as  $\Delta_{m_1} = -\Delta_{m_2} = 0.5J$ . Other parameters are the same as those used in Fig. 2.

SVFs, referred to as the double-squeezed configuration. Similar to the single-squeezed case, optimal entanglement is achieved when the SVFs are resonant with one of the supermodes, as shown in Figs. 3(a) and 3(b). Unlike the single-squeezed configuration, however, the two supermodes contribute equally to mediating entanglement. By appropriately tuning the cavity detunings, either supermode can be selectively activated to transfer quantum correlations from the SVFs to the magnon modes, as explicitly demonstrated in Figs. 3(c) and 3(d). This indicates that double entanglement channels can be selectively activated [see Fig. 1(d)]. The enhancement of the magnon-magnon entanglement arises because, although each SVF directly drives its corresponding cavity mode, the strong intercavity coupling allows the hybridized supermodes to be indirectly excited by both SVFs, giving rise to quantum interference at the interface of the activated supermode.

The interference effect is clearly seen in Fig. 4(a), where the upper supermode is activated as an example. The magnon-magnon entanglement can be tuned by the relative phases of the SVFs in the double-squeezed configuration: it is constructively enhanced when the two SVFs are in phase and completely suppressed when they are out of phase. This behavior contrasts with the single-squeezed configuration, where the entanglement

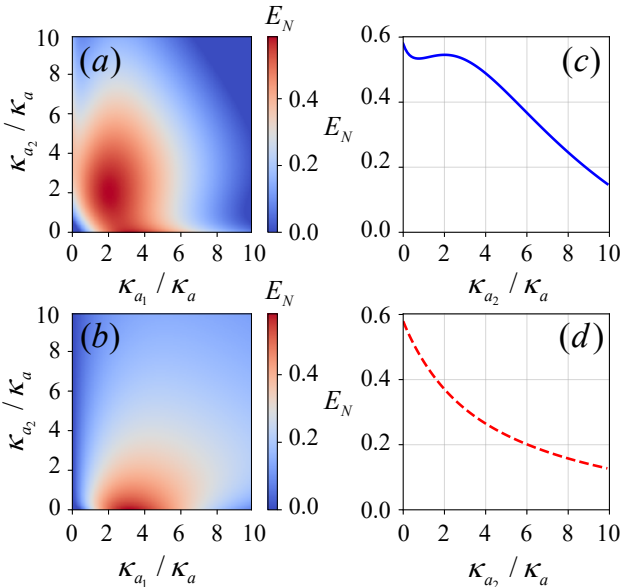


FIG. 5. The degree of magnon-magnon entanglement is shown as a function of the normalized decay rates of the two cavity modes for (a) the double-squeezed and (b) the single-squeezed configurations. Panels (c) and (d) display the corresponding cross-sectional results from (a) and (b), respectively, with  $\kappa_{a_1} = 2.5\kappa$  fixed. In all panels, the cavity detunings are set to  $\Delta_{a_1} = \Delta_{a_2} = -J$ , and the magnon detunings are set to  $\Delta_{m_1} = -\Delta_{m_2} = 0.5J$ . Other parameters are identical to those used in Fig. 2.

cannot be controlled by the local phase of a single SVF [Fig. 4(b)]. In both configurations, the entanglement can also be adjusted by the squeezing strength [Figs. 4(c) and 4(d)], indicating the existence of an optimal squeezing parameter for maximizing entanglement.

Furthermore, the double-squeezed configuration exhibits superior robustness against cavity decay. Strong magnon-magnon entanglement can be maintained for relatively large decay rates of cavity mode  $a_2$  [Fig. 5(a)], whereas in the single-squeezed configuration, significant entanglement requires extremely small decay rates [Fig. 5(b)], posing experimental challenges. As the decay rate increases, the entanglement decreases non-monotonically in the double-squeezed configuration [Fig. 5(c)], but monotonically in the single-squeezed case [Fig. 5(d)], further confirming the enhanced robustness of the double-squeezed setup.

Finally, we investigate the influence of bath temperature on the entanglement, as shown in Fig. 6. The double-squeezed configuration (blue solid curve) exhibits significantly greater tolerance to thermal noise compared with the single-squeezed configuration. Under feasible parameters, the entanglement survives up to  $\sim 450$  mK, whereas it decays around  $\sim 260$  mK in the single-squeezed case. Moreover, across the entire temperature range, the entanglement in the double-squeezed configuration remains consistently higher, confirming its superior robustness against thermal decoherence.

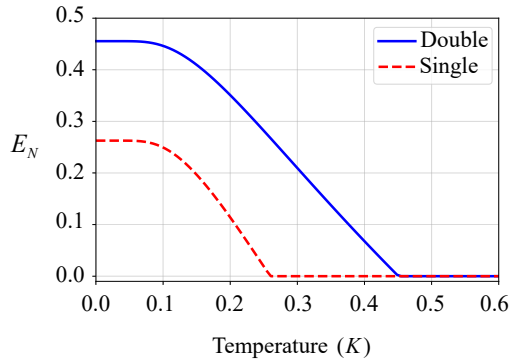


FIG. 6. The degree of magnon-magnon entanglement as a function of the bath temperature for both the double- and single-squeezed configurations, as respectively shown by the blue solid and red dashed curves. The cavity detunings are fixed at  $\Delta_{a_1} = \Delta_{a_2} = -J$ , and the magnon detunings are set to  $\Delta_{m_1} = -\Delta_{m_2} = 0.5J$ . Other parameters are the same as those used in Fig. 2.

rior robustness against thermal decoherence.

#### IV. CONCLUSION

In summary, we have presented a scheme to generate and enhance remote magnon-magnon entanglement in a coupled cavity-magnon system using only beam-splitter interactions. We show that when a single squeezed vacuum field drives one cavity mode, quantum correlations can only be transferred to two remote magnon modes through a *determined* supermode formed by the hybridized cavity modes, thereby establishing measurable entanglement between two magnon modes. In the double-squeezed configuration, where each cavity is driven by an independent squeezed field, both supermodes can be *selectively* activated by tuning the cavity detunings to transfer quantum correlations to the two magnon modes. In this case, two squeezed fields interfere coherently through the supermode interface, leading to a pronounced *enhancement* of magnon-magnon entanglement. This quantum interference further enables active phase control of the entanglement and markedly improves its robustness against thermal noise. Under experimentally realistic parameters, the entanglement survival temperature increases from approximately 260 mK in the single-squeezed case to about 450 mK in the double-squeezed case. Our work establishes a versatile and controllable approach to enhancing quantum correlations through double-squeezed-field interference, opening new avenues to study and enhance macroscopic quantum physics in cavity-magnon systems with only beam-splitter interactions.

This work was supported by the Zhejiang Province Key R&D Program of China (Grant No. 2025C01028), Natural Science Foundation of Zhejiang Province (Grant No.

LY24A040004), and Shenzhen International Quantum

Academy (Grant No. SIQA2024KFKT010).

---

[1] A. Prabhakar and D. D. Stancil, *Spin waves: Theory and applications* (Springer, 2009).

[2] J. Van Kranendonk and J. Van Vleck, Rev. Mod. Phys. **30**, 1 (1958).

[3] Y. Li, W. Zhang, V. Tyberkevych, W.-K. Kwok, A. Hoffmann, and V. Novosad, J. Appl. Phys. **128**, 130902 (2020).

[4] B. Z. Rameshti, S. V. Kusminskiy, J. A. Haigh, K. Usami, D. Lachance-Quirion, Y. Nakamura, C.-M. Hu, H. X. Tang, G. E. Bauer, and Y. M. Blanter, Phys. Rep. **979**, 1 (2022).

[5] H. Yuan, Y. Cao, A. Kamra, R. A. Duine, and P. Yan, Phys. Rep. **965**, 1 (2022).

[6] H. Huebl, C. W. Zollitsch, J. Lotze, F. Hocke, M. Greifenstein, A. Marx, R. Gross, and S. T. Goennenwein, Phys. Rev. Lett. **111**, 127003 (2013).

[7] Y. Tabuchi, S. Ishino, A. Noguchi, T. Ishikawa, R. Yamazaki, K. Usami, and Y. Nakamura, Science **349**, 405 (2015).

[8] X. Zhang, C.-L. Zou, L. Jiang, and H. X. Tang, Science advances **2**, e1501286 (2016).

[9] X. Zhang, C.-L. Zou, N. Zhu, F. Marquardt, L. Jiang, and H. X. Tang, Nat. Commun. **6**, 8914 (2015).

[10] D. Zhang, X.-Q. Luo, Y.-P. Wang, T.-F. Li, and J. Q. You, Nat. Commun. **8**, 1368 (2017).

[11] X. Zhang, K. Ding, X. Zhou, J. Xu, and D. Jin, Phys. Rev. Lett. **123**, 237202 (2019).

[12] J. Zhao, Y. Liu, L. Wu, C.-K. Duan, Y.-X. Liu, and J. Du, Phys. Rev. Appl. **13**, 014053 (2020).

[13] A. V. Sadovnikov, A. A. Zyablovsky, A. V. Dorofeenko, and S. A. Nikitov, Phys. Rev. Appl. **18**, 024073 (2022).

[14] H. Liu, D. Sun, C. Zhang, M. Groesbeck, R. Melaughlin, and Z. V. Vardeny, Sci. Adv. **5**, aax9144 (2019).

[15] Y. Cao and P. Yan, Phys. Rev. B **99**, 214415 (2019).

[16] L. Bai, M. Harder, P. Hyde, Z. Zhang, C.-M. Hu, Y. Chen, and J. Q. Xiao, Phys. Rev. Lett. **118**, 217201 (2017).

[17] Y.-P. Wang, J. Rao, Y. Yang, P.-C. Xu, Y. Gui, B. Yao, J. Q. You, and C.-M. Hu, Phys. Rev. Lett. **123**, 127202 (2019).

[18] M. Harder, B. Yao, Y. Gui, and C.-M. Hu, J. Appl. Phys. **129**, 201101 (2021).

[19] J. Rao, P. Xu, Y. Gui, Y. Wang, Y. Yang, B. Yao, J. Dietrich, G. Bridges, X. Fan, D. Xue, *et al.*, Nat. Commun. **12**, 1933 (2021).

[20] D. Xu, X.-K. Gu, H.-K. Li, Y.-C. Weng, Y.-P. Wang, J. Li, H. Wang, S.-Y. Zhu, and J. Q. You, Phys. Rev. Lett. **130**, 193603 (2023).

[21] D. Xu, X.-K. Gu, Y.-C. Weng, H.-K. Li, Y.-P. Wang, S.-Y. Zhu, and J. Q. You, Quantum Science and Technology **9**, 035002 (2024).

[22] G. Adesso and F. Illuminati, Journal of Physics A: Mathematical and Theoretical **40**, 7821 (2007).

[23] D. Bouwmeester, A. Ekert, and A. Zeilinger, *The Physics of Quantum Information* (Springer, Berlin, 2000).

[24] S. Haroche, Physics today **51**, 36 (1998).

[25] J. Li, S.-Y. Zhu, and G. Agarwal, Phys. Rev. Lett. **121**, 203601 (2018).

[26] J. Li and S.-Y. Zhu, New J Phys. **21**, 085001 (2019).

[27] M. Yu, H. Shen, and J. Li, Phys. Rev. Lett. **124**, 213604 (2020).

[28] J. Li and S. Gröblacher, Quantum Science and Technology **6**, 024005 (2021).

[29] D. Vitali, S. Gigan, A. Ferreira, H. Böhm, P. Tombesi, A. Guerreiro, V. Vedral, A. Zeilinger, and M. Aspelmeyer, Phys. Rev. Lett. **98**, 030405 (2007).

[30] J. Chen, X.-G. Fan, W. Xiong, D. Wang, and L. Ye, Phys. Rev. B **108**, 024105 (2023).

[31] Q.-G. Chen, M.-Y. Liu, X.-X. Huang, J. Chen, and W. Xiong, Chaos, Solitons & Fractals **202**, 117472 (2026).

[32] Z. Zhang, M. O. Scully, and G. S. Agarwal, Phys. Rev. Res. **1**, 023021 (2019).

[33] G. Zhang, Y. Wang, and J. You, Science China Physics, Mechanics & Astronomy **62**, 1 (2019).

[34] Y.-P. Wang, G.-Q. Zhang, D. Zhang, X.-Q. Luo, W. Xiong, S.-P. Wang, T.-F. Li, C.-M. Hu, and J. Q. You, Phys. Rev. B **94**, 224410 (2016).

[35] Y.-P. Wang, G.-Q. Zhang, D. Zhang, T.-F. Li, C.-M. Hu, and J. Q. You, Phys. Rev. Lett. **120**, 057202 (2018).

[36] M. Bi, X. Yan, Y. Zhang, and Y. Xiao, Phys. Rev. B **103**, 104411 (2021).

[37] R.-C. Shen, J. Li, Z.-Y. Fan, Y.-P. Wang, and J. Q. You, Phys. Rev. Lett. **129**, 123601 (2022).

[38] W. Xiong, M. Tian, G.-Q. Zhang, and J. Q. You, Phys. Rev. B **105**, 245310 (2022).

[39] M.-L. Peng, M. Tian, X.-C. Chen, G.-Q. Zhang, H.-C. Li, and W. Xiong, arXiv e-prints , arXiv (2023).

[40] R.-C. Shen, J. Li, Y.-M. Sun, W.-J. Wu, X. Zuo, Y.-P. Wang, S.-Y. Zhu, and J. You, Nat. Commun. **16**, 5652 (2025).

[41] X.-C. Chen, Z.-J. Wang, S.-B. Zheng, J. Chen, and W. Xiong, arXiv preprint arXiv:2509.01884 (2025).

[42] G. Liu, W. Xiong, and Z.-J. Ying, Phys. Rev. A **108**, 033704 (2023).

[43] G.-Q. Zhang, Z. Chen, W. Xiong, C.-H. Lam, and J. Q. You, Phys. Rev. B **104**, 064423 (2021).

[44] G.-Q. Zhang, S.-Y. Lin, W. Feng, Y.-H. Kang, and W. Xiong, arXiv preprint arXiv:2509.25985 (2025).

[45] J. Chen, X.-G. Fan, W. Xiong, D. Wang, and L. Ye, Phys. Rev. A **109**, 043512 (2024).

[46] M.-Y. Liu, Y. Gong, J. Chen, Y.-W. Wang, and W. Xiong, Chinese Physics B **34**, 057202 (2025).

[47] X.-H. Fan, Y.-N. Zhang, J.-P. Yu, M.-Y. Liu, W.-D. He, H.-C. Li, and W. Xiong, Adv. Quantum Tech. **7**, 2400043 (2024).

[48] X.-H. Fan, Q.-G. Chen, J. Chen, and W. Xiong, arXiv preprint arXiv:2508.09725 (2025).

[49] G.-Q. Zhang, Y. Wang, and W. Xiong, Phys. Rev. B **107**, 064417 (2023).

[50] K. Jähne, C. Genes, K. Hammerer, M. Wallquist, E. Polzik, and P. Zoller, Phys. Rev. A **79**, 063819 (2009).

[51] S. Huang and G. Agarwal, New Journal of Physics **11**, 103044 (2009).

[52] M. Yu, S.-Y. Zhu, and J. Li, Journal of Physics B: Atomic, Molecular and Optical Physics **53**, 065402

(2020).

[53] J. M. Nair and G. Agarwal, *Appl. Phys. Lett.* **117** (2020).

[54] Z.-B. Yang, X.-D. Liu, X.-Y. Yin, Y. Ming, H.-Y. Liu, and R.-C. Yang, *Phys. Rev. Appl.* **15**, 024042 (2021).

[55] K. Ullah, M. T. Naseem, and Ö. E. Müstecaplıoğlu, *Phys. Rev. A* **110**, 063715 (2024).

[56] N. Roch, M. E. Schwartz, F. Motzoi, C. Macklin, R. Vijay, A. W. Eddins, A. N. Korotkov, K. B. Whaley, M. Sarovar, and I. Siddiqi, *Phys. Rev. Lett.* **112**, 170501 (2014).

[57] D. F. Walls and G. Milburn, *Quantum optics* (Springer, Berlin, 1994).

[58] B. Yurke, *Journal of the Optical Society of America B* **4**, 1551 (1987).

[59] B. Yurke, P. Kaminsky, R. Miller, E. Whittaker, A. Smith, A. Silver, and R. Simon, *Phys. Rev. Lett.* **60**, 764 (1988).

[60] B. Yurke, L. Corruccini, P. Kaminsky, L. Rupp, A. Smith, A. Silver, R. Simon, and E. Whittaker, *Phys. Rev. A* **39**, 2519 (1989).

[61] R. Movshovich, B. Yurke, P. Kaminsky, A. Smith, A. Silver, R. Simon, and M. Schneider, *Phys. Rev. Lett.* **65**, 1419 (1990).

[62] M. A. Castellanos-Beltran, K. Irwin, G. Hilton, L. Vale, and K. Lehnert, *Nat. Phys.* **4**, 929 (2008).

[63] T. Yamamoto, K. Inomata, M. Watanabe, K. Matsuba, T. Miyazaki, W. D. Oliver, Y. Nakamura, and J. Tsai, *Appl. Phys. Lett.* **93** (2008).

[64] F. Mallet, M. Castellanos-Beltran, H. Ku, S. Glancy, E. Knill, K. Irwin, G. Hilton, L. Vale, and K. Lehnert, *Phys. Rev. Lett.* **106**, 220502 (2011).

[65] K. G. Fedorov, L. Zhong, S. Pogorzalek, P. Eder, M. Fischer, J. Goetz, E. Xie, F. Wulschner, K. Inomata, T. Yamamoto, *et al.*, *Phys. Rev. Lett.* **117**, 020502 (2016).

[66] S. Kono, Y. Masuyama, T. Ishikawa, Y. Tabuchi, R. Yamazaki, K. Usami, K. Koshino, and Y. Nakamura, *Phys. Rev. Lett.* **119**, 023602 (2017).

[67] A. Bienfait, P. Campagne-Ibarcq, A. Kiilerich, X. Zhou, S. Probst, J. Pla, T. Schenkel, D. Vion, D. Estève, J. Morton, *et al.*, *Phys. Rev. X* **7**, 041011 (2017).

[68] K. Murch, S. Weber, K. Beck, E. Ginossar, and I. Siddiqi, *Nature* **499**, 62 (2013).

[69] C. W. Gardiner and M. J. Collett, *Phys. Rev. A* **31**, 3761 (1985).

[70] Y. Tabuchi, S. Ishino, T. Ishikawa, R. Yamazaki, K. Usami, and Y. Nakamura, *Phys. Rev. Lett.* **113**, 083603 (2014).

[71] G. Vidal and R. F. Werner, *Phys. Rev. A* **65**, 032314 (2002).

[72] M. B. Plenio, *Phys. Rev. Lett.* **95**, 090503 (2005).

[73] R. Simon, *Phys. Rev. Lett.* **84**, 2726 (2000).